Neuron
Article

RIM Proteins Activate Vesicle Priming by Reversing Autoinhibitory Homodimerization of Munc13

Lunbin Deng,[1,3] Pascal S. Kaeser,[1,3] Wei Xu,[1,2] and Thomas C. Südhof[1,2,*]
[1]Department of Molecular and Cellular Physiology
[2]Howard Hughes Medical Institute
Stanford University, Lorry Lokey Building, 265 Campus Drive, Stanford, CA 94305-5453, USA
[3]These authors contributed equally to this work
*Correspondence: tcs1@stanford.edu
DOI 10.1016/j.neuron.2011.01.005

SUMMARY

At a synapse, the presynaptic active zone mediates synaptic vesicle exocytosis. RIM proteins are active zone scaffolding molecules that—among others—mediate vesicle priming and directly or indirectly interact with most other essential presynaptic proteins. In particular, the Zn^{2+} finger domain of RIMs binds to the C_2A domain of the priming factor Munc13, which forms a homodimer in the absence of RIM but a heterodimer with it. Here, we show that RIMs mediate vesicle priming not by coupling Munc13 to other active zone proteins as thought but by directly activating Munc13. Specifically, we found that the isolated Zn^{2+} finger domain of RIMs autonomously promoted vesicle priming by binding to Munc13, thereby relieving Munc13 homodimerization. Strikingly, constitutively monomeric mutants of Munc13 rescued priming in RIM-deficient synapses, whereas wild-type Munc13 did not. Both mutant and wild-type Munc13, however, rescued priming in Munc13-deficient synapses. Thus, homodimerization of Munc13 inhibits its priming function, and RIMs activate priming by disrupting Munc13 homodimerization.

INTRODUCTION

Neurotransmission is initiated when synaptic vesicles undergo exocytosis at the active zone, thereby releasing their neurotransmitter contents (Katz, 1969). Synaptic vesicle exocytosis is highly regulated, consistent with its role as the gatekeeper of neurotransmission (Stevens, 2003). Each event of exocytosis is induced by an action potential that induces Ca^{2+} influx via Ca^{2+} channels located in or near the active zone. The efficacy of action-potential-induced exocytosis depends on at least three parameters: the local activity of voltage-gated Ca^{2+} channels, the number of release-ready vesicles, and the Ca^{2+} sensitivity of these vesicles. Remarkably, none of the proteins that mediate these parameters (i.e., Ca^{2+} channels, the presynaptic fusion machinery composed of SNARE and SM proteins, and the Ca^{2+} sensor synaptotagmin) is exclusively localized to the active zone. Instead, their functions are organized at presynaptic release sites by the protein components of active zones (Südhof, 2004; Wojcik and Brose, 2007).

Among active zone protein components, RIM proteins are arguably the most central elements (Mittelstaedt et al., 2010). RIMs directly or indirectly interact with all other active zone proteins (Wang et al., 2000, 2002; Betz et al., 2001; Schoch et al., 2002; Ohtsuka et al., 2002; Ko et al., 2003), Ca^{2+} channels (Hibino et al., 2002; Kiyonaka et al., 2007; Kaeser et al., 2011), and the synaptic vesicle proteins Rab3 and synaptotagmin-1 (Wang et al., 1997; Coppola et al., 2001; Schoch et al., 2002). Consistent with a central role for RIMs in active zones, RIM proteins are essential for presynaptic vesicle docking, priming, Ca^{2+} channel localization, and plasticity (Koushika et al., 2001; Schoch et al., 2002, 2006; Castillo et al., 2002; Calakos et al., 2004; Weimer et al., 2006; Gracheva et al., 2008; Kaeser et al., 2008, 2011; Fourcaudot et al., 2008; Han et al., 2011). However, apart from recent progress in understanding the role of RIMs in vesicle docking and in localizing Ca^{2+} channels to active zones (Gracheva et al., 2008; Schoch et al., 2006; Kaeser et al., 2008, 2011; Han et al., 2011), it remains unclear how RIMs perform their functions. This gap in our understanding arose in part because multiple RIM isoforms are coexpressed in vertebrates, creating redundancy (Wang and Südhof, 2003), and because presynaptic rescue experiments require expression of rescue proteins in all neurons that are being analyzed, which is technically difficult for large proteins like RIMs.

One of the best documented phenotypes in RIM-deficient neurons is a strong reduction in vesicle priming (Koushika et al., 2001; Schoch et al., 2002; Calakos et al., 2004; Kaeser et al., 2008, 2011; Han et al., 2011). Priming activates synaptic vesicles for exocytosis, thereby creating the readily releasable pool (RRP) of vesicles. However, the nature of priming in general, and of the role of RIMs in priming in particular, remains unknown; even the relation of priming to docking—the process that physically attaches vesicles to the active zone as analyzed by electron microscopy—is unclear. In pioneering work, Rosenmund and Stevens (1996) showed that vesicles in the RRP can be induced to undergo exocytosis by application of hypertonic sucrose, which triggers vesicle fusion by a Ca^{2+}-independent, nanomechanical mechanism. Although the nonphysiological nature of the sucrose stimulus limits its usefulness (e.g., see Wu and Borst, 1999; Moulder and Mennerick, 2005),

measurements of vesicle pool sizes using this stimulus have been successfully applied as an operational definition of the RRP in many studies (e.g., see Basu et al., 2005; Betz et al., 2001; Rosenmund et al., 2002). Here, we also employ this approach, with the understanding that the operational definition of the RRP as the sucrose-stimulated vesicle pool includes both docking and priming since the two processes cannot be separated (Xu-Friedman et al., 2001).

The synaptic vesicle membrane fusion machinery is composed of SNARE and SM proteins and constitutes a central element of priming; in addition, multiple other priming proteins have been characterized. Among these, the most important besides RIMs are likely Munc13s, which are multidomain proteins of active zones that are essential for all synaptic vesicle priming and additionally participate in shaping short-term synaptic plasticity (Brose et al., 1995; Augustin et al., 1999a; Rosenmund et al., 2002). Munc13s most likely function by interacting with SNARE proteins (Betz et al., 1997; Basu et al., 2005; Madison et al., 2005; Stevens et al., 2005; Guan et al., 2008); interestingly, they also directly bind to RIMs (Betz et al., 2001; Schoch et al., 2002; Dulubova et al., 2005). Most RIM isoforms contain an N-terminal Zn^{2+} finger domain that binds to the N-terminal C_2A domain of the Munc13 isoforms Munc13-1 and ubMunc13-2. Importantly, the Munc13 C_2A domain (which does not bind Ca^{2+}, different from synaptotagmin C_2 domains but similar to RIM C_2 domains) forms a tight homodimer in the absence of the RIM Zn^{2+} finger; binding of the RIM Zn^{2+} finger to the Munc13 C_2A domain converts this homodimer into a RIM/Munc13 heterodimer (Dulubova et al., 2005; Lu et al., 2006). Furthermore, the Zn^{2+} finger domain of RIMs is flanked by α-helical sequences that bind to Rab3 (Wang et al., 1997). Thus, the N-terminal sequence of RIMs can mediate simultaneous binding of RIMs to Munc13 as a priming factor and to Rab3 as a vesicle GTP-binding protein (Dulubova et al., 2005).

Together, the structural and genetic data on the Munc13/RIM/Rab3 complex prompted the hypothesis that RIMs activate synaptic vesicle priming by recruiting Munc13 to the active zone and stabilizing it there and that the crucial function of RIMs is to colocalize Munc13 with synaptic vesicles via their N-terminal sequences and with other active zone proteins and Ca^{2+} channels via their C-terminal sequences (Wang et al., 1997, 2000, 2002; Betz et al., 2001; Schoch et al., 2002; Ohtsuka et al., 2002; Ko et al., 2003; Andrews-Zwilling et al., 2006; Kaeser et al., 2008, 2011). In the present paper, we have tested this hypothesis using rescue experiments with newly generated conditional double-knockout (DKO) mice targeting all major presynaptic RIM isoforms (Kaeser et al., 2011). Unexpectedly, we find that RIMs do not act during vesicle priming as classical scaffolding proteins, i.e., that their mechanism of action does not require the close colocalization of target proteins. Instead, we show that the isolated RIM Zn^{2+} finger domain is sufficient for activating priming, and that it functions by binding to Munc13, thereby disrupting Munc13 homodimers. Specifically, we show that mutant, constitutively monomeric forms of Munc13 can reverse the priming deficiency in RIM-deficient synapses, whereas wild-type Munc13 cannot, but strikingly both mutant monomeric and wild-type Munc13 rescue priming in Munc13-deficient synapses. Thus, RIMs switch on Munc13's priming function by disrupting the autoinhibitory homodimerization of Munc13.

RESULTS

RIM Deletion Reduces the Priming Capacity of Active Zones

We recently generated conditional DKO mice in which cre-recombinase deletes expression of all multidomain presynaptic RIM isoforms (i.e., RIM1α, 1β, 2α, 2β, and 2γ; Kaeser et al., 2011). To explore how RIMs function in synaptic vesicle priming, we cultured hippocampal neurons from conditional RIM DKO mice and infected them either with a lentivirus expressing inactive mutant (control) or active wild-type EGFP-tagged cre-recombinase (referred to as cDKO neurons). Measurements of spontaneous excitatory and inhibitory "mini" synaptic events (mEPSCs and mIPSCs, respectively) showed that the frequency of mEPSCs and mIPSCs was decreased more than 10- and more than 3-fold, respectively, in RIM-deficient neurons, whereas their amplitudes were unchanged (Figures 1A and 1B). This finding supports previous data that RIMs are essential for a normal presynaptic release probability in excitatory and inhibitory synapses (Schoch et al., 2002, 2006; Calakos et al., 2004; Kaeser et al., 2008, 2011; Han et al., 2011; see also Figure S1, available online). Thus, in the following, we analyzed only inhibitory synaptic transmission that does not exhibit network activity and is easier to evaluate in cultured neurons (Maximov et al., 2007).

Assessments of the RRP in RIM-deficient cDKO neurons with a 30 s application of hypertonic sucrose uncovered a more than 4-fold decrease in the RRP size (Figure 1C). Hypertonic sucrose induces an initial release transient that corresponds to the RRP and then transitions into a steady-state phase that corresponds to the continuous stimulation of the exocytosis of vesicles refilling the RRP (Rosenmund and Stevens, 1996). Comparison of release triggered during the initial transient (i.e., the first 10 s of sucrose application) or during the steady-state phase (i.e., the last 15 s of the application) revealed that the RIM deletion suppressed both phases equally (Figure 1C). Plots of the cumulative charge transfer showed that the kinetics of sucrose-induced release were unchanged (Figure 1D). These findings indicate that the RIM deletion decreased the total capacity of the RRP but not its steady-state refilling rate.

Measurements of the levels of active zone proteins and of other essential presynaptic proteins in RIM-deficient neurons uncovered only a single major change: a decrease in Munc13-1 levels in the cDKO neurons lacking all presynaptic RIM isoforms (Figure 1E), with the decrease in Munc13-1 levels observed here being slightly larger (67%) than that observed previously in brains from mice lacking only RIM1α (~60%)(Schoch et al., 2002). Thus, deletion of RIMs does not produce a global change in the composition of the release machinery but a discrete change in one particular interacting protein, Munc13.

We next characterized the dynamics of the RRP in RIM-deficient synapses. Measurements of the refilling of the RRP after sucrose-induced depletion, with a second sucrose stimulus applied at variable interstimulus intervals, showed that although the RRP in RIM-deficient synapses is massively reduced, its

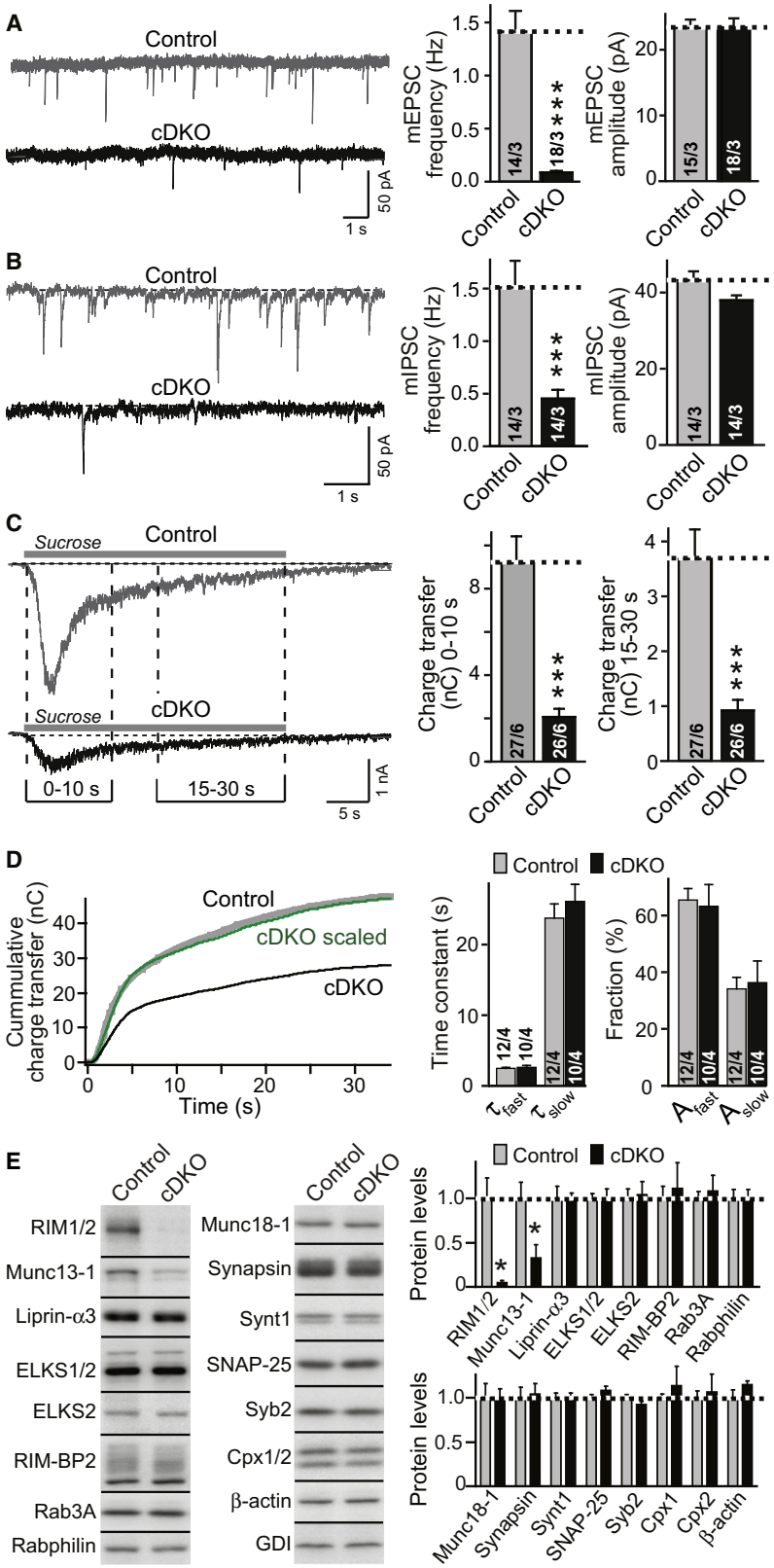

Figure 1. Conditional Deletion of RIM1α, 1β, 2α, 2β, and 2γ Dramatically Decreases the RRP Size

All experiments in this and most of the following figures employ hippocampal neurons cultured from conditional RIM1/2 DKO mice that were infected with lentiviruses expressing inactive (Control) or active cre-recombinase (cDKO).

(A and B) Sample traces (left) and summary graphs (right) of the frequency and amplitude of spontaneous miniature excitatory (mEPSCs) and inhibitory postsynaptic currents (mIPSCs), monitored in control (gray) and RIM-deficient cDKO hippocampal neurons (black).

(C) Sample traces (left) and summary graphs (right, as charge transfer) of inhibitory postsynaptic currents induced by hypertonic sucrose (0.5 M) in control (gray) and RIM-deficient cDKO (black) neurons. Hypertonic sucrose was puffed onto the patched neuron for 30 s in the presence of 1 μM TTX, 10 μM CNQX, and 50 μM APV. Charge transfer during the initial (0–10 s) and the steady-state responses (15–30 s of application) were quantified to estimate the RRP size and the RRP recovery rate, respectively.

(D) Cumulative charge transfer (left) and kinetic analyses of the cumulative charge transfer (right) of sucrose-induced postsynaptic currents in control (gray) and RIM-deficient cDKO neurons (black). The integrated charge transfer was fitted by a double-exponential function to determine kinetic parameters for the fast and the slow component (τ_{fast}, A_{fast} and τ_{slow}, A_{slow}, respectively).

(E) Sample immunoblots (left) and protein quantitations (right) of control and cDKO neurons.

Data shown are means ± SEMs (numbers in bars indicated numbers of cells and cultures analyzed). Statistical significance was assessed by Student's t test (*$p < 0.05$; ***$p < 0.001$). For short-term synaptic plasticity, see Figure S1.

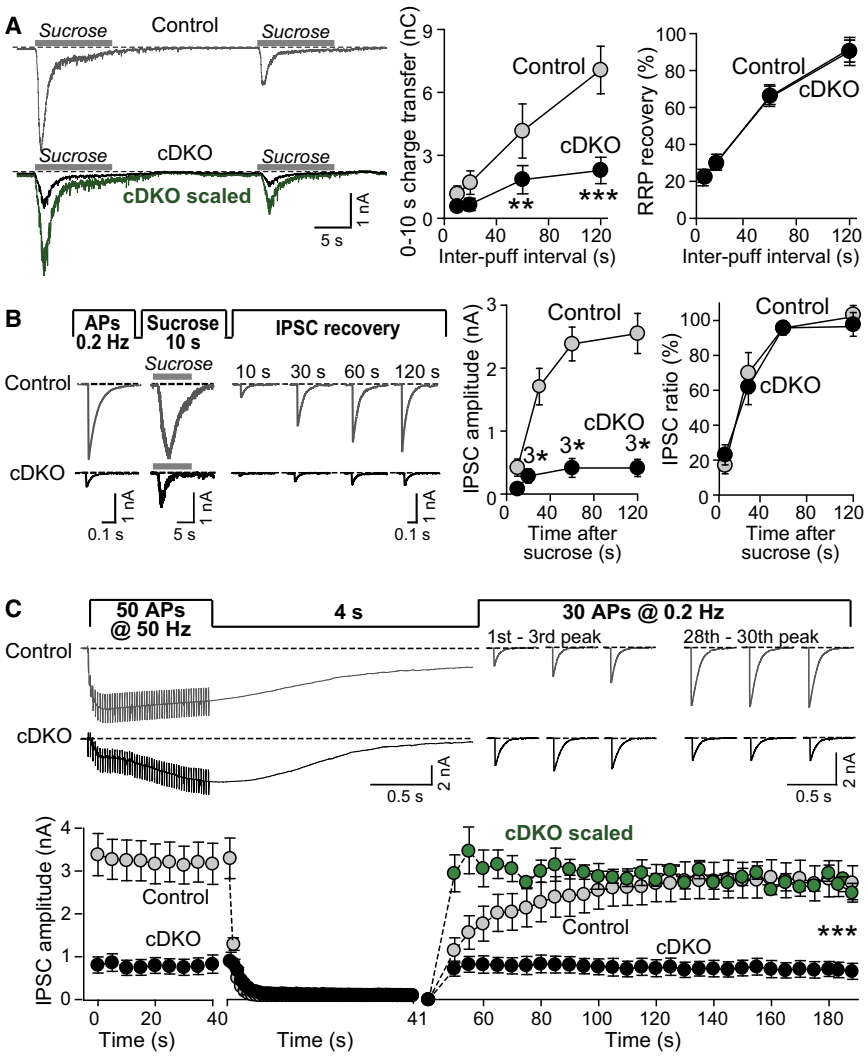

Figure 2. Differential Effects of the RIM Deletion on RRP Capacity and Refilling Rates

(A) Representative IPSC traces (left) and summary graphs (right, showing absolute and normalized data) of the RRP recovery as a function of the inter-puff interval between two sucrose applications, applied at increasing interstimulus intervals (10, 20, 60, and 120 s). RRP recovery was calculated by dividing the second sucrose-induced charge transfer by the first; in the right graph, the resulting ratio was normalized to that observed at the 120 s interval.

(B) Sample traces (left) and summary data (right, showing absolute and normalized data) of the recovery rate of single evoked IPSCs after sucrose-induced RRP depletion. IPSC amplitudes were measured at multiple time points after RRP depletion (10, 30, 60, 120 s), and normalized to control IPSC amplitudes before RRP depletion.

(C) Sample traces (top) and summary graph of the IPSC amplitudes (bottom) measured in cDKO and control neurons during depletion of the RRP by a 50 Hz stimulus train applied for 1 s and during the recovery from the RRP depletion after the train. The stimulation protocol is outlined on top; neurons were stimulated with ten pulses at 0.2 Hz before the high-frequency train. For the responses in RIM-deficient cDKO neurons, both absolute and normalized data are shown. For expanded views of IPSCs during the high-frequency train and an analysis of the delayed release kinetics, see Figure S2.

Data shown are means ± SEMs. Statistical significance was assessed by 2-way ANOVA (**$p < 0.01$; ***$p < 0.001$). p values and numbers are listed in Table S2.

relative refilling rate is unchanged (Figure 2A). We then used a more physiological stimulus for monitoring the RRP recovery after sucrose-induced depletion and applied isolated action potentials at increasing intervals after RRP depletion (Figure 2B). Again, RIM-deficient synapses exhibited a normal relative rate of recovery after sucrose depletion.

Finally, we examined the recovery of synaptic responses after the RRP had been depleted by a 50 Hz stimulus train applied for 1 s (Figure 2C). The amount of release triggered during the stimulus train appeared decreased in RIM-deficient synapses, consistent with a decrease in the RRP, and no synaptic responses were detectable at the end of the train in either control or RIM-deficient synapses (Figure S2A), suggesting that the RRP was depleted.

During the initial recovery period, control and RIM-deficient cDKO neurons exhibited an identical absolute recovery rate of inhibitory postsynaptic currents (IPSCs) and an increased relative recovery rate. After the initial period, however, the IPSCs in control neurons continued to increase because their RRP was not yet refilled, whereas the IPSCs in RIM-deficient neurons exhibited no further increase, presumably because their smaller RRP was already full after a short recovery period (Figure 2C). These results suggest that the RRP in RIM-deficient synapses refills relatively faster after depletion with a stimulus train than after depletion by hypertonic sucrose, possibly because the Ca^{2+}-dependent acceleration of vesicle priming is relatively more effective in the RIM-deficient synapses.

The RIM Zn^{2+} Finger Acts Autonomously in Synaptic Vesicle Priming

A plausible hypothesis is that RIM acts in vesicle priming via Munc13, the dominant priming factor in the presynaptic active zone (Augustin et al., 1999a; Varoqueaux et al., 2002). RIM proteins bind to Munc13 via their Zn^{2+} finger domain (Betz et al., 2001; Schoch et al., 2002; Dulubova et al., 2005); binding is mediated by two critical lysine residues in the RIM Zn^{2+} finger domain (K144 and K146) whose mutation blocks Munc13 binding (Dulubova et al., 2005; Lu et al., 2006). To ensure that the Zn^{2+} finger is the only RIM sequence that binds to Munc13, we examined the interaction of ubMunc13-2 with wild-type

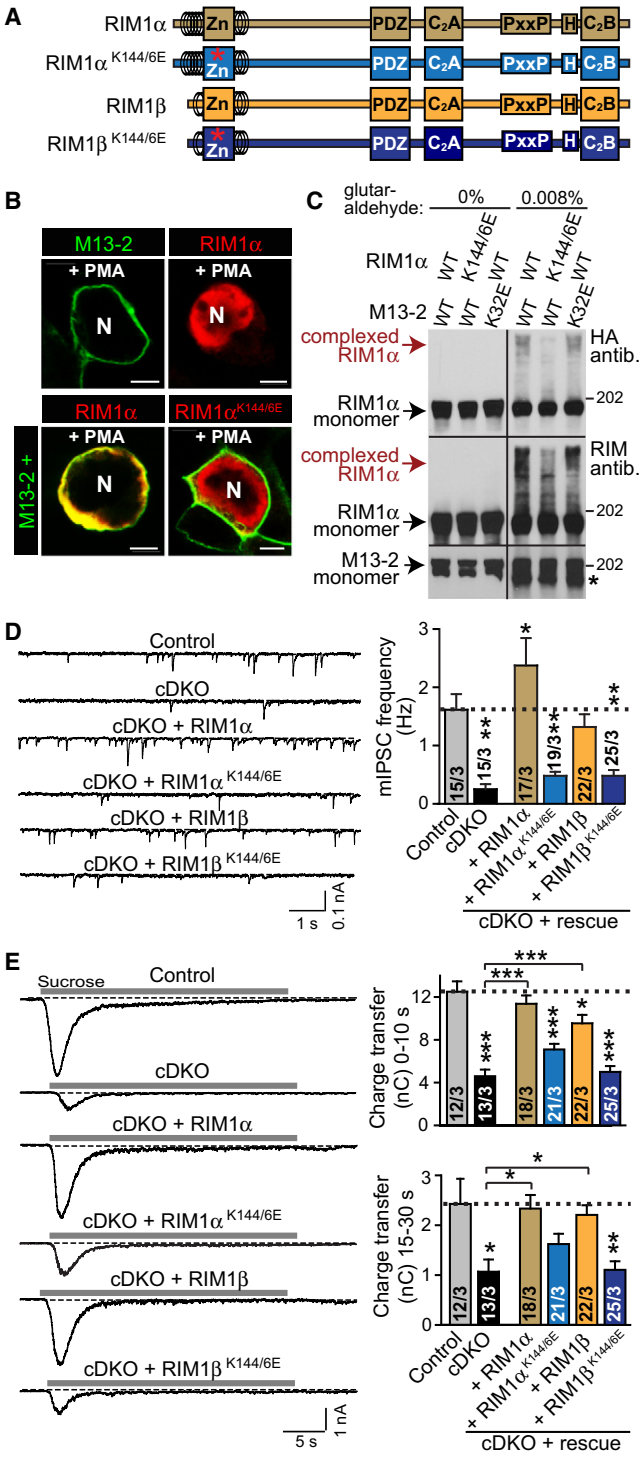

Figure 3. RIM N-Terminal Domains Mediate Synaptic Vesicle Priming

(A) Diagram of full-length wild-type and mutant RIM1α and RIM1β rescue proteins expressed in RIM-deficient cDKO neurons via an IRES sequence from the same mRNA as cre-recombinase (asterisk = K144/6E substitution).

(B) Localization of wild-type or K144/6E mutant RIM1α and ubMunc13-2 in transfected HEK293 cells. RIMs and ubMunc13-2 were transfected either alone (top) or in combination, and their colocalization was studied after translocation of Munc13 by phorbol ester (PMA) to the plasma membrane. Note that without Munc13 binding, RIM1α is sequestered into the nucleus in nonneuronal cells but recruited to the plasma membrane in the presence of ubMunc13-2 and PMA (N is an abbreviation for nucleus. The scale bar represents 5 μm).

(C) Crosslinking of wild-type or K144/6E mutant RIM1α with Munc13s. HEK293 cells expressing the indicated proteins were treated in control solution or solution containing 0.008% glutaraldehyde, and proteins were analyzed by SDS-PAGE and immunoblotting with antibodies against the HA-tag of RIM1α or against the central domains of RIM (R809). ubMunc13-2 monomer was detected with antibodies against the mVenus tag (* indicates an unspecific band). Note that we included as a control the K32E mutant of ubMunc13-2 that does not homodimerize but retains RIM binding (see Lu et al., 2006). The high-molecular weight bands are not clearly resolved on the blot, probably because of their large size and variable degrees of crosslinking.

(D) Sample traces (left) and summary graphs of the frequency (right) of spontaneous mIPSCs monitored in control and RIM-deficient cDKO neurons with or without RIM rescue.

(E) Sample traces (left) and summary graphs of the RRP size as measured by the initial sucrose response (right, top) and of the steady-state refilling size (right, bottom) in control neurons, and cDKO neurons with or without rescue. Rescue efficacies are shown in Figure S3 and Table S3.

Data shown are means ± SEMs (numbers in bars indicated numbers of cells and cultures analyzed). Statistical significance was assessed by one-way ANOVA (*p < 0.05; **p < 0.01; ***p < 0.001).

and mutant RIM1α in transfected HEK293 cells by imaging the Munc13-dependent recruitment of RIM1α to the membrane (Figure 3B) or by crosslinking studies (Figure 3C). We used a RIM1α mutant that contains glutamate substitutions in the two lysine residues of the Zn^{2+} finger domain that are critical for Munc13 binding (the K144/6E mutation) (Dulubova et al., 2005). Furthermore, we used the ubMunc13-2 isoform of Munc13 because this isoform was characterized best in previous rescue experiments (e.g., see Rosenmund et al., 2002; Junge et al., 2004; Shin et al., 2010). Both the imaging and the crosslinking experiments showed that full-length wild-type RIM1α was tightly bound to ubMunc13-2 via its Zn^{2+} finger domain, whereas the Zn^{2+} finger domain mutants of full-length RIM1α were not, indicating that the only RIM sequence that binds to ubMunc13-2 is the RIM Zn^{2+} finger domain (Figures 3B and 3C and Figure S3A). Note that chemical crosslinking of proteins by glutaraldehyde is an inherently low-efficiency technique that depends on the precise distance of reactive groups in a protein complex and on the concentration of the crosslinking agent. As a result, the degree of RIM-Munc13 crosslinking observed here does not reflect the stoichiometry of the RIM/Munc13 complex, and the crosslinking data are most meaningfully interpreted as the differences between the wild-type and mutant RIM and Munc13 proteins, as evidenced by the loss of high-molecular weight crosslinked proteins with mutant RIM1α$^{K144/6E}$ that does not bind to Munc13. In contrast to crosslinking results, colocalization in the imaging results does give a representation of how much of the RIM and Munc13 proteins are in a true complex, suggesting that there is stoichiometric binding for the wild-type but not mutant proteins (Figures 3B and 3C).

We then tested whether Munc13 binding by the RIM Zn^{2+} finger domain is required for RIM-dependent vesicle priming by expressing rescue proteins in RIM-deficient neurons. Wild-type RIM1α and RIM1β reversed the decrease in

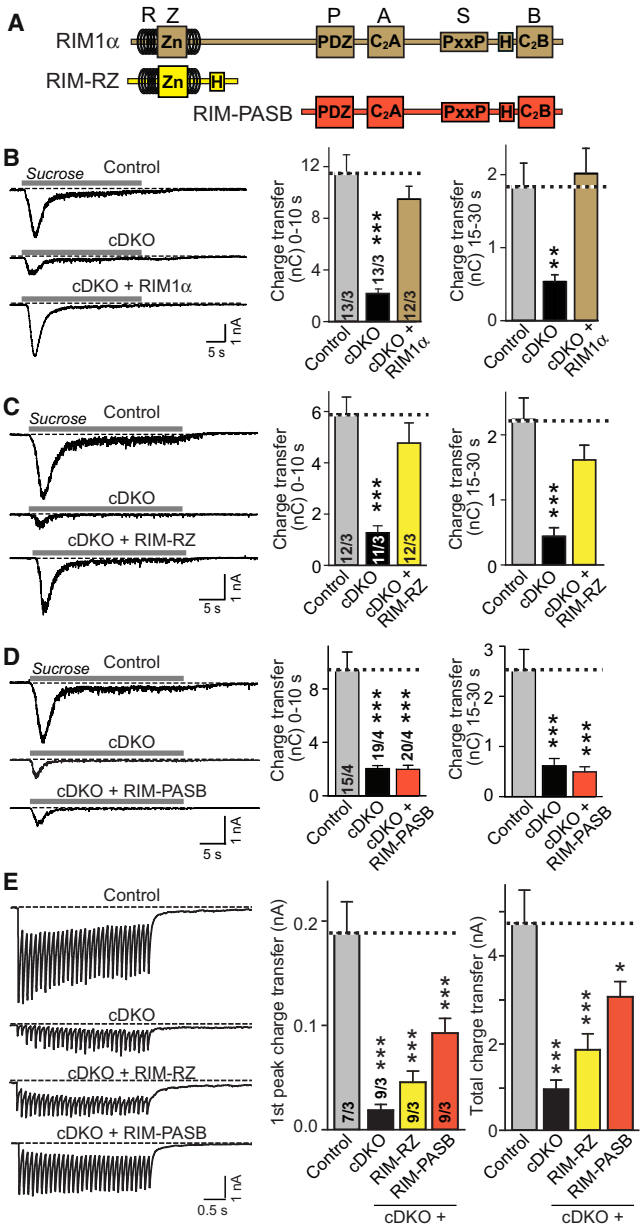

Figure 4. RIM N-Terminal Domains Are Necessary and Sufficient for Priming

(A) Diagram of full-length RIM1α and of RIM1α fragments expressed as rescue proteins in RIM-deficient cDKO neurons via an IRES sequence from the same mRNA as cre-recombinase. The single-letter code above the RIM1α diagram identifies the various domains (The following abbreviations are used: R, Rab3-binding α-helical region; Z, Munc13-binding Zn^{2+} finger region; P, PDZ domain; A, C_2A domain; S, proline-rich SH3-binding PxxP motif; B, C_2B domain); H marks the presence of a human influenza hemagglutinin (HA)-tag. (B–D) Sample traces (left) and summary graphs of initial and steady-state RRP sizes in control or RIM-deficient cDKO neurons without or with rescue with RIM1α (B), RIM-RZ (C), or RIM-PASB (D).

(E) Analysis of IPSCs evoked by a 10 Hz stimulus train in control neurons, RIM-deficient cDKO neurons without rescue, or RIM-deficient cDKO neurons rescued with the RIM-RZ or the RIM-PASB fragment. Note that unlike sucrose-evoked release, action-potential-induced release is partly rescued by both RIM fragments.

spontaneous minirelease in RIM-deficient neurons; in fact, RIM1α appeared to even enhance spontaneous release (Figure 3D). The Zn^{2+} finger domain mutation in RIM1α and RIM1β, however, impaired rescue. Moreover, RIM1α and RIM1β both rescued the impairment in sucrose-induced release in RIM-deficient neurons; again, the Zn^{2+} finger mutation partly blocked this rescue in RIM1α and completely in RIM1β (Figure 3E and Figure S3C). Overall, these experiments indicate that in RIM proteins, the Zn^{2+} finger domain is the major effector domain for priming; moreover, the experiments show that RIM1α may mediate rescue more efficiently than RIM1β, consistent with the notion that the N-terminal Rab3-binding activity of RIM1α (which is absent from RIM1β; Kaeser et al., 2008) contributes to release.

We next asked whether the RIM Zn^{2+} finger requires the context of other C-terminal domains of RIM to promote priming, as would be expected for a scaffolding protein, or whether it acts autonomously. We examined rescue with RIM1α fragments composed of either only its N-terminal Rab3- and Munc13-binding sequences (referred to as the RIM-RZ fragment), or of its C-terminal fragment containing the PDZ, C_2A, and C_2B domains and the RIM-BP-binding sequence (referred to as the RIM-PASB fragment; Figure 4A). Surprisingly, the N-terminal RIM-RZ fragment was sufficient to rescue vesicle priming in RIM-deficient neurons, whereas the C-terminal PASB-fragment had no rescue effect (Figures 4B–4D; note that the RIM-PASB fragment efficiently rescues the Ca^{2+} influx impairment in RIM-deficient neurons [Kaeser et al., 2011]). Importantly, the N-terminal RIM-RZ fragment did not significantly alter vesicle priming when overexpressed in wild-type neurons (Figure S4). Unlike release induced by hypertonic sucrose, both the N-terminal and the C-terminal RIM1α fragment increased release stimulated by a 10 Hz train of action potentials (Figure 4E). This result is consistent with completely separated roles of the N-terminal RIM domains in vesicle priming and of the C-terminal RIM domains in boosting local Ca^{2+} influx (Kaeser et al., 2011).

The rescue of priming in RIM-deficient neurons by the RIM-RZ fragment alone is surprising because it suggests that RIM does not act as a classical scaffolding protein that functions by recruiting multiple other proteins via its N- and C-terminal domains to the same subcellular location. However, the RIM-RZ fragment still binds to two proteins in a trimeric complex—Rab3 and Munc13 (Dulubova et al., 2005). Thus, its rescue activity could either be mediated by coupling Rab3 on synaptic vesicles to Munc13 in the active zone or it could be because of autonomous functions of each of its binding activities.

To distinguish between these two possibilities, we systematically eliminated Rab3 and Munc13 binding from the RIM-RZ fragment, the former by using the equivalent fragment from RIM1β that lacks Rab3 binding (RIM-Z) and the latter by introducing the Zn^{2+} finger mutations into the RIM-RZ and RIM-Z

Data shown are means ± SEMs (numbers in bars indicated numbers of cells and cultures analyzed). Statistical significance was assessed by one-way ANOVA (**p < 0.01; ***p < 0.001). For an analysis of the effect of RIM-RZ expression in wild-type neurons, see Figure S4; numerical values are shown in Table S4.

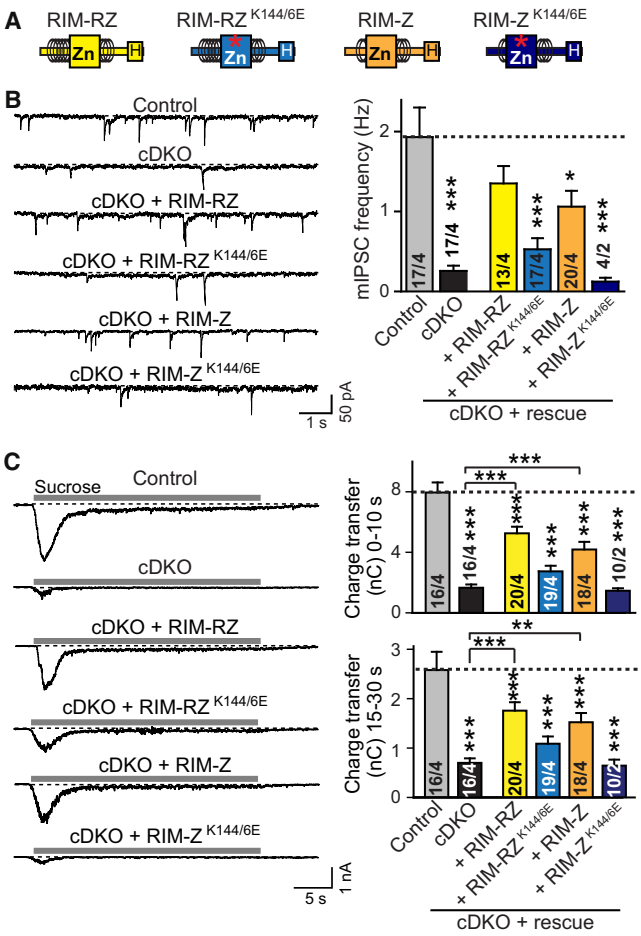

Figure 5. Munc13 Binding by the N-Terminal RIM Zn^{2+} Finger Domain Autonomously Activates Vesicle Priming

(A) Diagram of N-terminal wild-type and mutant RIM fragments expressed as rescue proteins in cDKO neurons via an IRES sequence from the same mRNA as cre-recombinase (asterisk = K144/6E substitution).

(B) Sample traces (left) and summary graph (right) of the frequency of spontaneous mIPSCs monitored either in control neurons and cDKO neurons with or without rescue.

(C) Sample traces (left) and summary graphs (right) of RRP size in control neurons and cDKO neurons with or without rescue. Rescue efficacies are indicated in Figure S5 and Table S5.

Data shown are means ± SEMs (numbers in bars indicated numbers of cells and cultures analyzed). Statistical significance was assessed by one-way ANOVA (*$p < 0.05$; **$p < 0.01$; ***$p < 0.001$).

fragments (Figure 5A). Rescue experiments with these fragments showed that both the RIM-RZ and the RIM-Z fragment rescued ~40%–60% of the decrease in spontaneous (Figure 5B) and sucrose-evoked release (Figures 5C and Figure S5), whereas the Zn^{2+} finger mutations blocked part of the rescue in RIM-RZ and all of the rescue in the RIM-Z fragment. Thus, the isolated Rab3- and Munc13-binding domains of RIMs act as autonomous switches to activate priming, and their actions are independent of each other and additive, with the RIM Zn^{2+} finger domain having a bigger effect on spontaneous release and RRP size than the RIM Rab3-binding domain.

Constitutively Monomeric Mutant of Munc13 Rescues Loss of Priming in RIM-Deficient Neurons

The unexpected ability of the isolated RIM Zn^{2+} finger to activate priming in RIM-deficient neurons indicates that RIMs prime vesicle fusion by an autonomous effect of their Zn^{2+} finger and suggests that the Zn^{2+} finger promotes priming by converting an autoinhibitory Munc13 C_2A domain homodimer into an active Zn^{2+} finger/C_2A domain heterodimer (Figure 6A). However, other mechanisms of action for the Zn^{2+} finger are also possible; for example, the RIM Zn^{2+} finger could bind to other, as yet unidentified, targets, or binding of the RIM Zn^{2+} finger to Munc13 may induce other downstream effects in addition to disrupting the C_2A domain homodimer.

The hypothesis that the RIM Zn^{2+} finger domain promotes priming by disrupting Munc13 homodimers predicts that constitutively monomeric Munc13 should be able to rescue the impairment of priming observed in RIM-deficient neurons, which would not be the case if the RIM Zn^{2+} finger bound to other targets or produced other effects on Munc13. Thus, to test this hypothesis, we expressed in RIM-deficient neurons wild-type ubMunc13-2 (as a control) and mutant ubMunc13-2 that is constitutively monomeric (to examine the role of Munc13 monomerization by the RIM Zn^{2+} finger). We chose a previously characterized Munc13 point mutation (K32E) that does not interfere with RIM binding by Munc13 but converts the Munc13 C_2A domain into a constitutive monomer (Lu et al., 2006, Figure 6A).

Expression of wild-type Munc13 had no significant effect on the decreased minifrequency in cDKO neurons, but mutant, constitutively monomeric Munc13 rescued ~50% of the impairment (Figure 6B). Strikingly, when we measured the RRP using hypertonic sucrose, wild-type Munc13 overexpression again had no significant rescue effect, but the constitutively monomeric Munc13 mutant nearly completely rescued the decrease in the RRP in RIM-deficient neurons (Figure 6C and Figure S6A). Overexpression of wild-type or mutant ubMunc13-2 in wild-type neurons did not significantly alter the minifrequency and RRP size (Figures 6B and 6C, right). Immunostaining with pan-Munc13 or ubMunc13-2 antibodies confirmed that both wild-type and mutant, constitutively monomeric Munc13 were similarly expressed and partially localized to synapsin-positive presynaptic terminals (Figure 6D). Immunoblotting and quantitative RT-PCR further showed that there were no significant differences in expression levels of the two Munc13 constructs (Figures S6B and S6C). Together, these data show that the differential rescue effects of wild-type and mutant Munc13 are a function of Munc13 monomerization and are not due to differences in expression levels and/or synaptic targeting. Thus, a mutation that renders Munc13 constitutively monomeric serves as a second-site suppressor of the RIM deletion phenotype, bypassing the requirement for RIM in vesicle priming.

Does the rescue with wild-type or constitutively monomeric mutant Munc13 restore physiological synaptic responses and does it alter the Ca^{2+} sensitivity of release? To address this question, we measured action-potential-evoked IPSCs as a function of the extracellular Ca^{2+} concentration (Figure 6E and Figures S6D–S6F). Again, expression of wild-type Munc13 had no detectable effect on the massive decrease in IPSC amplitudes produced by the RIM deletion, whereas expression of constitutively monomeric

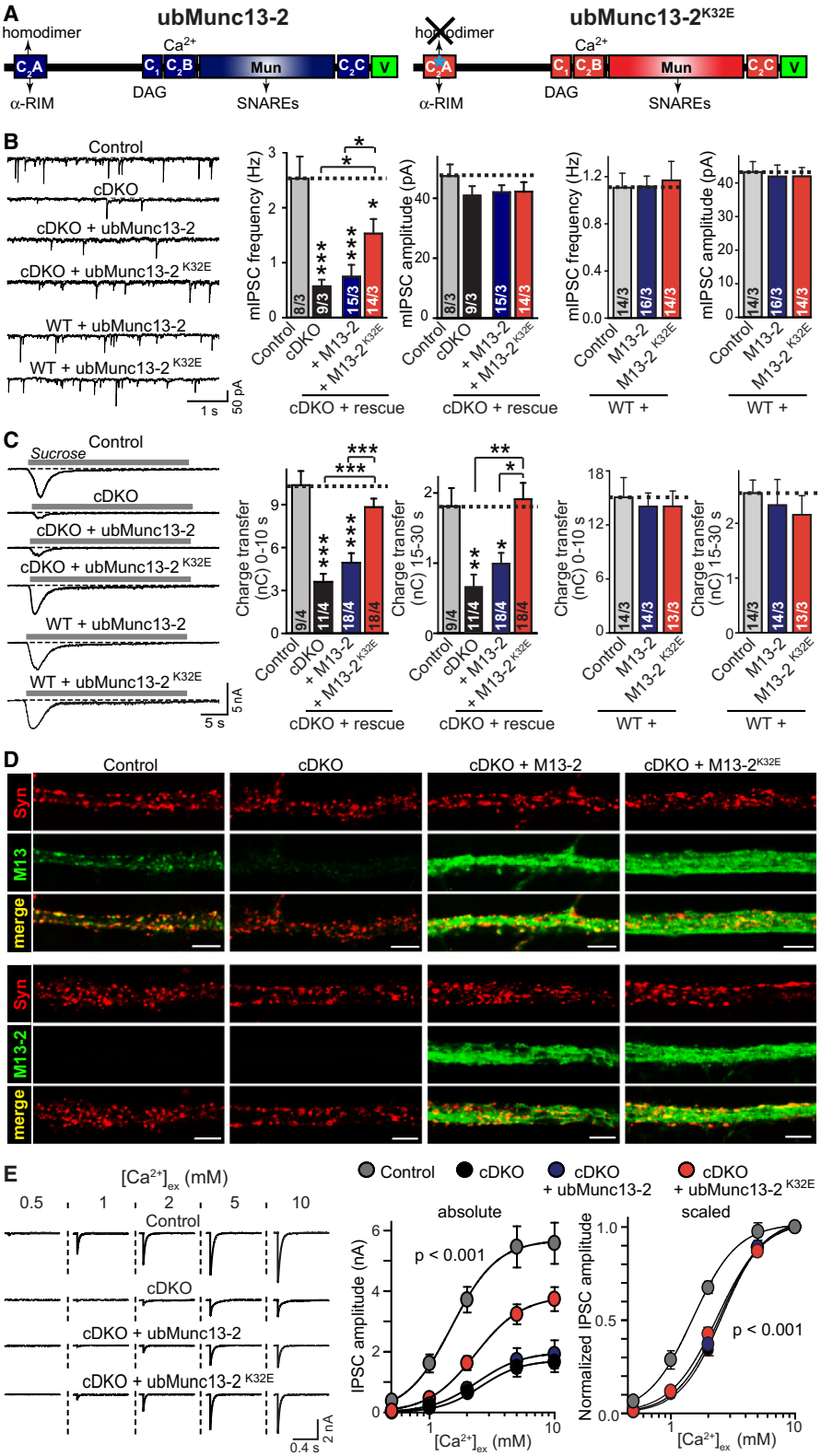

Figure 6. Constitutively Monomeric Mutant ubMunc13-2 Bypasses the Loss of Priming in RIM-Deficient Neurons

(A) Diagram of wild-type and mutant ubMunc13-2 rescue proteins expressed in cDKO neurons. Key domains of Munc13 (C_1 and C_2 domains and the MUN domain. V is an abbreviation for mVenus-tag) and their interactions are indicated (DAG is an abbreviation for diacylglycerol). Cre-recombinase and Munc13s

mutant Munc13 rescued approximately half of the decrease in synaptic responses induced by deletion of RIMs (Figure 6E), similar to the rescue of the mIPSC frequency (Figure 6B). When we analyzed the Ca^{2+} dependence of the IPSCs by fitting the data to a Hill function, mutant or wild-type Munc13 had no effect on the decreased apparent Ca^{2+} affinity of release induced by the RIM deletion (Figures 6E and Figure S6D). This result supports the notion that the impaired Ca^{2+} channel localization in RIM-deficient synapses is not restored by overexpression of constitutively monomeric or wild-type Munc13 because the Ca^{2+} channel localization depends on a direct interaction of RIM with Ca^{2+} channels (Kaeser et al., 2011), which is independent of Munc13.

So far, our data suggest that RIMs promote vesicle priming by disrupting the Munc13 C_2A-homodimer. However, it is possible that the Munc13 C_2A domain performs an additional function that is activated when it is released from the homodimer, i.e., that it is not the homodimer per se that is inhibitory but that the homodimer occludes a critical additional activity of the C_2A domain. To test this possibility, we investigated a truncation mutant of Munc13 that lacks the C_2A domain and thus cannot mediate any C_2A-domain-dependent activity, including homodimerization (referred to as ubMunc13-$2^{\Delta C2A}$; Figure 7A). Experiments in transfected HEK293 cells confirmed that as expected, this N-terminally truncated Munc13 mutant does not interact with RIM1α nor does it form homodimers (Figures 7B and 7C and Figure S7A). This Munc13 mutant also largely rescued the minifrequency (Figure 7D) and entirely reversed the loss of vesicle priming in RIM-deficient neurons (Figure 7E). Thus, monomeric Munc13 does not require its N-terminal C_2A domain to rescue the priming impairment in RIM-deficient neurons, and the C_2A domain thus probably acts to inhibit the Munc13 priming function by homodimerization, which is reversed by RIM.

Wild-Type and Monomeric Munc13 Rescue Priming in Munc13-Deficient Synapses

In RIM-deficient cDKO neurons, Munc13 levels are reduced by 67% (Figure 1E). Our data show, however, that RIMs do not mediate priming by simply stabilizing Munc13 levels since wild-type Munc13 cannot rescue the RIM deficiency phenotype. Instead, we find that RIMs act by activating Munc13 and suggest furthermore that the major function of the Munc13 C_2A domain is to autoinhibit Munc13 function by homodimerization in the absence of RIM, with the autoinhibition being reversed when RIMs disrupt the homodimerization. However, it is possible that the Munc13 C_2A domain performs additional RIM-independent functions in release that would be mediated in our rescue experiments by the continued presence of wild-type Munc13 in the RIM-deficient neurons. To test this possibility, we characterized the ability of wild-type and mutant ubMunc13-2 to rescue the reduced priming observed in neurons with strong reductions in total Munc13 levels. If our conclusions were correct, both wild-type and monomeric ubMunc13-2 should rescue priming in these neurons because RIM is present to monomerize wild-type Munc13 and because mutant ubMunc13-2^{K32E} lacking homodimerization should be constitutively active. Furthermore, monomeric mutant ubMunc13-$2^{\Delta C2A}$ unable to bind RIMs should also rescue priming, in line with previous reports suggesting that the MUN domain of Munc13 is the minimal domain required for Munc13 mediated vesicle priming (Basu et al., 2005; Madison et al., 2005; Stevens et al., 2005).

To suppress Munc13 levels, we screened shRNAs against Munc13-1. We identified one shRNA (KD91) that strongly diminished Munc13-1 mRNA and protein levels (Figures 8A and 8B; ~80% knockdown [KD] efficiency). We then cultured neurons from constitutive Munc13-2 KO mice (Varoqueaux et al., 2002) and infected them either with lentiviruses expressing the Munc13-1 KD shRNA or with empty control lentiviruses in addition to lentiviruses expressing rescue proteins (Figures S8A–S8C).

Munc13-deficient neurons exhibited a significant decrease in minifrequency and RRP size (Figures 8C–8F). Both parameters were rescued by re-expression of wild-type ubMunc13-2, of mutant ubMunc13-2^{K32E} containing the C_2A domain point mutation, or of mutant ubMunc13-$2^{\Delta C2A}$ in which the C_2A domain is deleted (Figures 8C–8F, and Figures S8D–S8E). These data rule out nonspecific effects during the rescue of priming in RIM-deficient neurons by the various Munc13 mutants, and—more importantly—confirm that RIMs serve as a molecular switch that disrupts Munc13 homodimers in synaptic vesicle priming.

DISCUSSION

In the present study, we explore the mechanism of action of RIM and Munc13 proteins in synaptic vesicle priming. We make three principal observations that are unexpected in view of current ideas about RIM and Munc13 function and vesicle priming, namely (1) that the RIM Zn^{2+} finger domain activates priming autonomously as a switch not by mediating the coassembly of multiple proteins into a protein complex at the active zone, (2) that the RIM Zn^{2+} finger switches on priming by activating

were expressed from separate lentiviruses by consecutive infection (cre and control viruses at DIV3, Munc13 viruses at DIV5). Note that the K32E mutation of the Munc13 C_2A domain (Munc13^{K32E}) renders Munc13 constitutively monomeric (Lu et al., 2006).

(B) Sample traces (left) and summary graph (right) of the frequency of spontaneous mIPSCs monitored in control and RIM-deficient cDKO neurons with or without wild-type or mutant Munc13 expression (top 4 traces and left panels) or in wild-type neurons with Munc13 expression (bottom two traces and right panels).

(C) Sample traces (left) and summary graphs (right) of RRP size in control and cDKO neurons with or without rescue or in wild-type neurons with Munc13 expression.

(D) Confocal sections of cDKO neurons with or without rescue stained for all Munc13 isoforms (top) or for ubMunc13-2 (bottom) and counterstained with synapsin antibodies. Note that wild-type and mutant ubMunc13-2 rescue proteins exhibit similar levels and localizations.

(E) Expression of K32E mutant but not wild-type ubMunc13-2 partially rescues the amplitude of action-potential evoked IPSCs in RIM-deficient cDKO neurons but does not rescue their impaired Ca^{2+} responsiveness.

Data shown are means ± SEMs (numbers in bars indicated numbers of cells and cultures analyzed). Statistical significance was assessed by 1-way ANOVA (*$p < 0.05$; **$p < 0.01$; ***$p < 0.001$). For additional analyses and numerical data, see Figure S6 and Table S6.

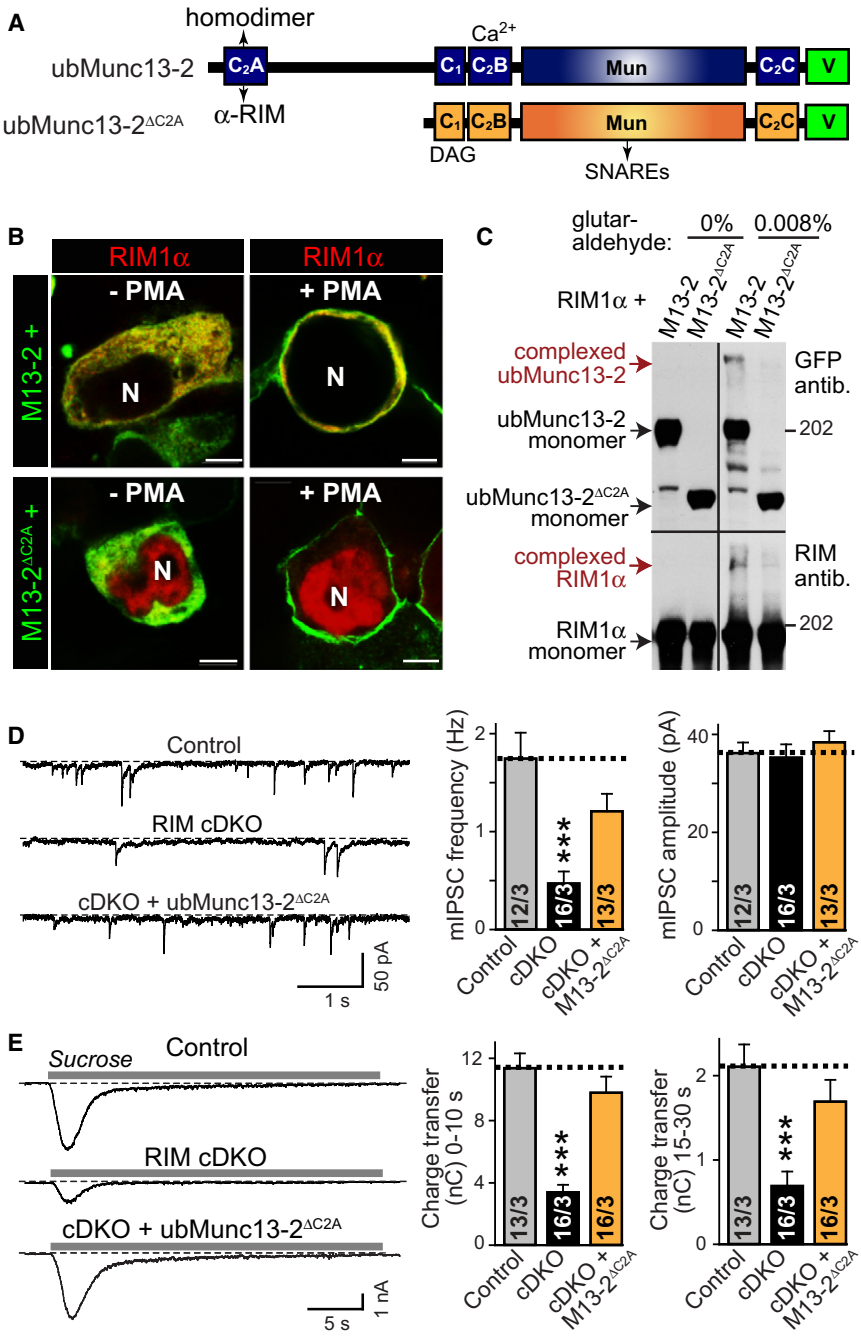

Figure 7. The ubMunc13-2 C_2A Domain Is Dispensable for Rescuing the RRP in RIM-Deficient Neurons

(A), Diagram of ubMunc13-2 rescue proteins expressed in cDKO neurons via an IRES sequence from the same mRNA as cre-recombinase. Key interactions of various domains are indicated.

(B) Colocalization of full-length RIMs and Munc13s in HEK293 cells depends on the Munc13 C_2A domain. RIM1α and wild-type or ΔC_2A mutant ubMunc13-2 were transfected into HEK293 cells and their colocalization was studied before (−PMA) or after phorbol ester-induced translocation (+PMA) of Munc13 to the plasma membrane. Note that without Munc13 binding (i.e., with ΔC_2A mutant ubMunc13-2), RIM is largely localized to nuclei in nonneuronal cells, whereas in the presence of wild-type ubMunc13-2, it is either cytosolic (−PMA) or on the plasma membrane (+PMA) (N is an abbreviation for nucleus; the scale bar represents 5 μm).

(C) Crosslinking of wild-type or ΔC_2A mutant ubMunc13-2 with RIM1α. HEK293 cells expressing the indicated proteins were treated in control solution or solution containing 0.008% glutaraldehyde, and proteins were analyzed by SDS-PAGE and immunoblotting with antibodies against the mVenus tag of Munc13 and the central domains of RIM (R809).

(D) Sample traces (left) and summary graph (right) of miniature mIPSCs monitored in control neurons and cDKO neurons with or without ubMunc13$^{\Delta C2A}$ expression.

(E) Sample traces (left) and summary graphs (right) of RRP size in control neurons and cDKO neurons with or without ubMunc13$^{\Delta C2A}$ rescue. Initial (left) and steady-state RRP sizes (right) are indicated. Data shown are means ± SEMs (numbers in bars indicated numbers of cells and cultures analyzed). Statistical significance was assessed by one-way ANOVA (***$p < 0.001$). For additional data, see Figure S7.

Munc13 and does so by disrupting constitutive Munc13 homodimers produced by their C_2A domain, and (3) that C_2A domain-mediated homodimerization of Munc13 inhibits its priming function in the absence of RIM but is disinhibited by the RIM Zn^{2+} finger (Figure 8G). Note that we refer to priming in a broad sense, defined operationally as the process that renders vesicles sensitive to stimulation by hypertonic sucrose, and do not attempt to differentiate between stages of vesicle docking and priming. The distinction between docking and priming is classically made by electron microscopy, but the case of Munc13 illustrates how tenuous this distinction can be. Although in traditional electron microscopy experiments no docking defect in Munc13-deficient synapses was observed (Augustin et al., 1999a; Varoqueaux et al., 2002), a recent study using high-pressure freezing reached the opposite conclusion (Siksou et al., 2009). It is unclear which of the two electron microscopy approaches renders a "true" picture; thus, we make no attempt to tease apart physical vesicle attachment (docking) and conversion of attached into release-ready vesicles (priming), but use the term "priming" in a generic sense as defined above.

RIMs Act in Priming as Molecular Switches Not as Scaffolds Mediating Coassembly of Multiple Proteins

Classical scaffolding molecules often act by producing the colocalization of multiple downstream effectors (Mishra et al.,

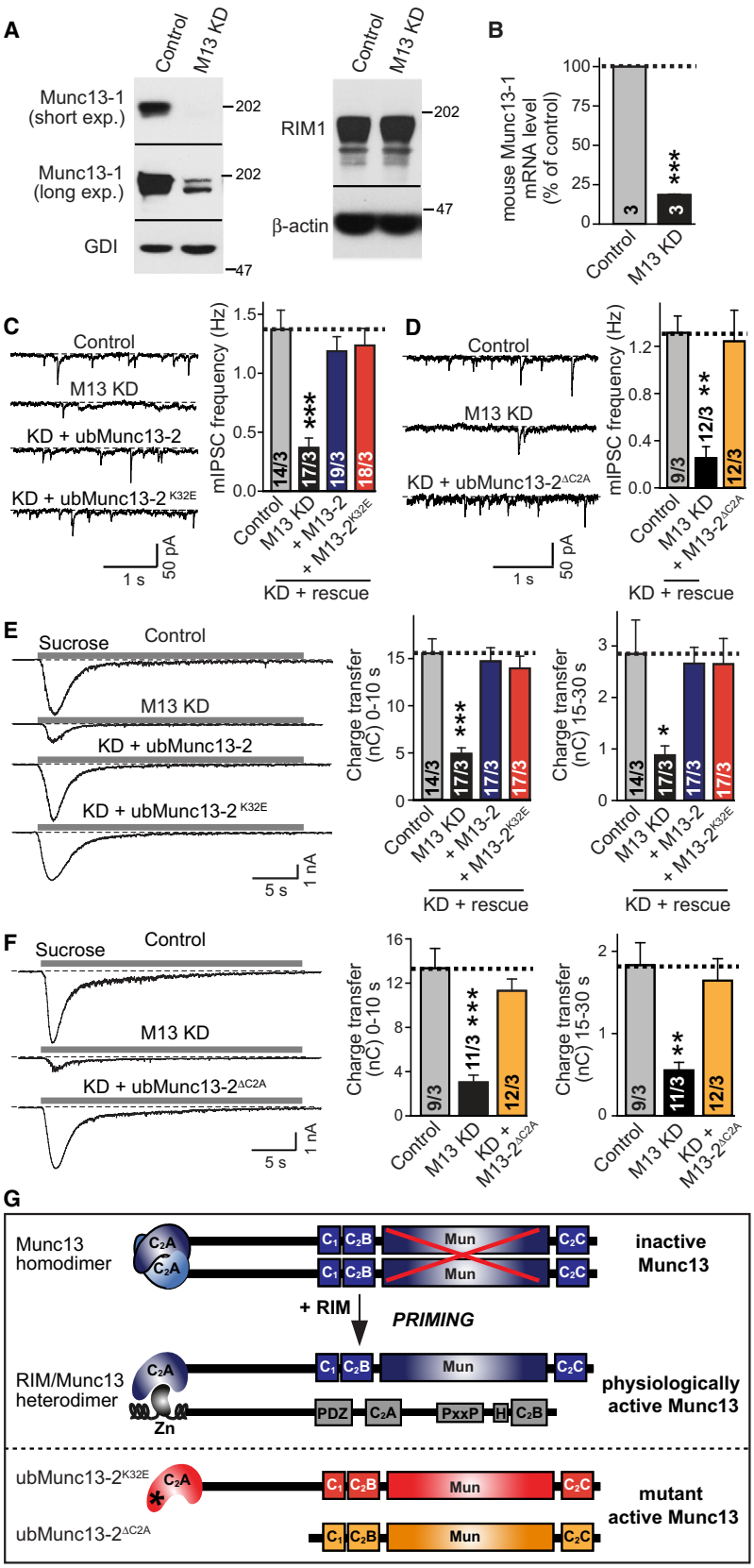

Figure 8. Wild-Type and Constitutively Monomeric Mutant ubMunc13-2 Rescue Priming in Munc13-Deficient Neurons

(A) Immunoblotting for Munc13-1 and control proteins in neurons from Munc13-2 KO mice infected with control lentiviruses or with the Munc13-1 KD virus. Neurons were consecutively infected with the Munc13 rescue or control lentiviruses at DIV3 and with the Munc13-1 KD or control lentiviruses at DIV5.

(B) Quantitative real-time RT-PCR measurements of the mRNA levels of Munc13-1 in control and Munc13-1 KD neurons.

(C and D) Sample traces (left) and summary graph (right) of the spontaneous mIPSC frequency monitored in control neurons and M13 KD neurons either with or without ubMunc13 or ubMunc13^{K32E} rescue (C) or ubMunc13$^{\Delta C2A}$ rescue (D). Data of mIPSC amplitudes are shown in Figure S7.

(E) Sample traces (left) and summary graphs (right) of RRP size in control neurons and Munc13 KD neurons with or without ubMunc13 rescue. Initial (left) and steady-state RRP sizes (right) are indicated.

(F) Sample traces (left) and summary graphs (right) of RRP size in control neurons, and Munc13 KD neurons with or without ubMunc13$^{\Delta C2A}$ rescue. Initial (left) and steady-state RRP sizes (right) are indicated.

(G) Model of the RIM priming switch. We propose that RIM activates priming by disrupting autoinhibitory Munc13 C_2A domain homodimers. The inactive Munc13 homodimer is physiologically activated by the RIM Zn^{2+} finger domain that converts the homodimer into a RIM/Munc13 heterodimer. This activation can be bypassed with constitutively monomeric mutant Munc13^{K32E} or Munc13 $^{\Delta C2A}$, but not with wild-type Munc13, in RIM-deficient neurons.

Data shown are means ± SEMs (numbers in bars indicated numbers of cells and cultures analyzed). Statistical significance was assessed by 1-way ANOVA (*$p < 0.05$; **$p < 0.01$; ***$p < 0.001$). For additional data, see Figure S8.

2007; Pawson and Scott, 2010). RIMs were presumed to act as scaffolds in this sense because of their domain structure (Schoch et al., 2002). However, we find that surprisingly, the RIM Zn^{2+} finger autonomously promotes vesicle priming by directly activating Munc13. With this observation, we revise our previous conclusions based on peptide injections into the calyx of Held synapse (Dulubova et al., 2005), which seemed to suggest that uncoupling the domains of RIM suppresses their function. The present genetic approach is a more definitive approach than peptide injections, as it does not depend on unphysiologically high protein levels to achieve a dominant-negative effect but utilizes rescue of a loss-of-function state as an assay. It seems likely that the high peptide concentrations used previously produce unintended effects unrelated to the normal function of RIM, illustrating the general difficulty of interpreting experiments in which a protein fragment is introduced into a wild-type synapse at high concentrations (Südhof, 2004).

If RIM proteins are not scaffolds for the coassembly of proteins into complexes, why do they have a multidomain structure? One possibility is that the autonomous function of the RIM Zn^{2+} finger domain in priming is subject to intramolecular regulation, which could be involved in the role of RIM in long-term presynaptic plasticity (Castillo et al., 2002; Chevaleyre et al., 2007; Fourcaudot et al., 2008; Kaeser et al., 2008). Another possibility is that assembly of the autonomous functions of different RIM domains into a single protein ensures the right relative activity of these domains, i.e., a constant ratio of their activities. A third possibility is that this arrangement may be economical in terms of organizing the expression and localization of so many activities mediated by different domains.

RIMs Switch on Priming by Disrupting Munc13 Homodimers

Crystal structures revealed that the Munc13 C_2A domain forms a tight homodimer with nanomolar affinity; this dimer is disrupted by binding of the RIM Zn^{2+} finger, resulting in Zn^{2+} finger/C_2A domain heterodimers (Dulubova et al., 2005; Lu et al., 2006). Our results suggest that Munc13 homodimerized by its C_2A domain is inactive in priming but activated by the RIM Zn^{2+} finger binding that disrupts the homodimer. The strongest evidence for this conclusion comes from the suppression of the priming phenotype in RIM-deficient synapses by mutant, constitutively monomeric Munc13, but not by wild-type Munc13 (Figures 6 and 7). Note that the constitutively monomeric Munc13 mutants rescued only the priming deficit of RIM-deficient neurons not their Ca^{2+}-triggering phenotype, which manifested in a ~50% rescue of synaptic strength in the RIM-deficient neurons by the mutant Munc13 (Figure 6E). Furthermore, whereas only mutant, constitutively monomeric Munc13 but not wild-type Munc13 rescued priming in RIM-deficient neurons, both mutant Munc13 and wild-type Munc13 rescued priming in Munc13-deficient neurons (Figure 8). An alternative hypothesis to the model proposed here is that an as yet unidentified protein binds to the Munc13 C_2A domain and inhibits Munc13 function and that this protein is displaced by the RIM Zn^{2+} finger. However, this hypothesis would require that the putative Munc13-binding protein has nanomolar affinity for Munc13 (since it has be stronger than Munc13 homodimerization) that it is nevertheless displaced from Munc13 by RIM. In addition, the putative Munc13-binding protein would be required to bind to the site of Munc13 homodimerization, effectively suppressing it because the C_2A domain would always be either bound to RIM or to the other protein. Viewed together, these improbable requirements render the alternative hypothesis highly unlikely and nonparsimonious.

The Munc13 C_2A Domain Functions as an Autoinhibitory Module that Blocks Priming by Homodimerization

The autoinhibitory function of the Munc13 C_2A domain is surprising since no other C_2 domain has been associated with a comparable function. Of four principal synaptic Munc13 isoforms (Munc13-1, ubMunc13-2, bMunc13-2, and Munc13-3), only the first two contain a C_2A domain (Brose et al., 1995; Augustin et al., 1999b; Koch et al., 2000), raising the question of how the other two Munc13 isoforms (which are less abundant) are regulated and whether they are possibly controlled by a different RIM-dependent mechanism. It seems likely that Munc13 acts on SNARE proteins in priming (Basu et al., 2005; Madison et al., 2005; Stevens et al., 2005; Guan et al., 2008), but the mechanisms of Munc13 function in priming, and of the inactivation of Munc13 function by homodimerization, remain unclear. One possibility is that homodimeric Munc13 is inherently unstable and becomes degraded in RIM-deficient neurons, thereby accounting for the priming phenotype and the reduced Munc13 levels in RIM-deficient neurons (Figure 1; Schoch et al., 2002). However, overexpression of wild-type Munc13 did not rescue the priming phenotype in RIM-deficient neurons, suggesting that simply increasing Munc13 levels is not sufficient to rescue priming in RIM-deficient synapses. Another possibility is that homodimeric Munc13 is not correctly targeted to synapses and becomes degraded if it is not in the correct location (Andrews-Zwilling et al., 2006; Kaeser et al., 2009). Although possible, this hypothesis appears rather unlikely given the rescue of the RIM- and Munc13-deficiency phenotypes by N-terminally truncated Munc13 (Figures 7 and 8), which suggests that Munc13 is transported to synapses without RIM proteins and without binding to RIM proteins. Independent of which explanation will turn out to be correct, the mechanism of Munc13 activation we identify here is opposite to what is classically observed for signal transduction events; dimerization is usually activating, whereas in our case it is inhibitory, suggesting a more diverse range of biological activation mechanisms than previously envisioned.

Outlook

The current study identifies a molecular mechanism involved in vesicle priming by the active zone but raises new questions. At a basic level, how is an active zone generated—what protein nucleates its assembly? The fact that the RIM Zn^{2+} finger alone is active suggests that it acts downstream of Munc13 targeting to active zones and cannot physically tether Munc13 to them; similarly, Munc13 is not essential for targeting other proteins to active zones and thus also not involved in their recruitment to active zones. Clearly, despite its central function, RIM alone does not organize the active zone, an activity that may be carried out by an overlapping set of several proteins instead of a single master regulator. Another important question is how RIM proteins contribute to long-term synaptic plasticity—is this

mediated by a coordination of their various functions or by one particular aspect? With the present results, we now know of two switches at the active zone that involve RIM and regulate synaptic neurotransmitter release: the GTP-dependent interaction of Rab3 with RIMs, and the Zn^{2+} finger mediated RIM-dependent monomerization of Munc13. Given the central roles of RIM and Rab3 in all known forms of long-term presynaptic plasticity (e.g., Castillo et al., 1997, 2002; Chevaleyre et al., 2007; Fourcaudot et al., 2008, Kaeser et al., 2008), a plausible hypothesis is that these switches could be regulated by synaptic activity and thus mediate such plasticity, an exciting hypothesis that would account for the enormous effects of presynaptic plasticity on neurotransmitter release.

EXPERIMENTAL PROCEDURES

Primary Hippocampal Cultures, Lentiviral Infections, and Rescue Constructs

High-density hippocampal cultures were prepared from newborn mice and infected with lentiviruses as described (Kaeser et al., 2009). The RIM1 rescue constructs were generated from rat RIM1α (Wang et al., 1997) or RIM1β (Kaeser et al., 2008) and are described in the Supplemental Experimental Procedures. The GFP-tagged rat ubMunc13-2 lentivirus was previously published (Rosenmund et al., 2002). In contrast to the RIM rescue constructs that were expressed bicistronically with an internal ribosome entry site (IRES sequence [Kaeser et al., 2009, 2011]), the Munc13-overexpression experiments were performed by superinfection of cre-infected cultures with Munc13-expressing lentiviruses.

Electrophysiology

Whole-cell patch-clamp recordings were performed in cultured hippocampal neurons at DIV13-15 as described (Maximov et al., 2007, Kaeser et al., 2009, Kaeser et al., 2008, Maximov et al., 2009). The extracellular solution contained (in mM) 140 NaCl, 4 KCl, 2 CaCl2, 2 MgCl2, 10 HEPES-NaOH (pH 7.3), and 10 glucose, with 315 mOsm. Glass pipettes (3–5 MΩ) were filled with an internal solution containing (in mM) 145 CsCl, 5 NaCl, 10 HEPES-CsOH (pH 7.3), 10 EGTA, 4 MgATP, and 0.3 Na2GTP, with 305 mOsm. mEPSCs and mIPSCs were recorded in the presence of 1 μM tetrodotoxin (TTX) plus either 50 μM picrotoxin and 50 μM APV (mEPSCs) or 10 μM CNQX and 50 μM D-APV (mIPSCs), respectively. For measurement of RRP, 0.5 M hypertonic sucrose was perfused with a picospritzer in the presence of 1 μM TTX (except for the experiments in Figure 2B, where TTX was omitted), 10 μM CNQX, and 50 μM D-APV. Ca^{2+} titration experiments were performed as described (Kaeser et al., 2011). RRP rescue efficacy was calculated according to following equation: % = (mean rescue charge transfer − mean cDKO charge transfer)/(mean control charge transfer − mean cDKO charge transfer) * 100, where the mean charge transfer is the average of sucrose-induced charges of neurons recorded in the same batch of culture. Data were acquired with a multiclamp 700B amplifier with pClamp9, sampled at 10 Hz, and filtered at 1 Hz. In all experiments, the experimenter was blind to the genotype.

Protein Quantitations in Neuronal Cultures

Neurons were harvested in a detergent free buffer, homogenized with a glass-teflon homogenizer, and spun at 256,000 × g for 30 min, and the pellet was used for protein quantitations. Protein contents were adjusted by use of a bicinchoninic (BCA) protein assay kit (Pierce Biotechnology). Twenty micrograms of protein was loaded per lane on standard SDS/Page gels for western blotting, ^{125}iodine-labeled secondary antibodies were used for detection as previously described (Kaeser et al., 2008), and valosin-containing protein (VCP), GDP dissociation inhibitor (GDI), and β-actin were used as internal standards.

Protein Interaction Assays

Munc13/RIM colocalization experiments in transfected HEK293T cells were performed as described (Andrews-Zwilling et al., 2006). Crosslinking experiments were performed in transfected HEK293T cells and were induced with 0.008% glutaraldehyde after membrane recruitment of Munc13 with phorbol esters. Detailed experimental protocols are in the Supplemental Information.

Immunofluorescence Staining of Cultured Neurons

Cultured neurons were fixed in 4% paraformaldehyde/phosphate-buffered saline, permeabilized in 0.1% Triton X-100/3% bovine serum albumin/phosphate-buffered saline, and incubated overnight with anti-Munc13 rabbit polyclonal antibodies (antibody 41, 1:2000) or anti-ubMunc13-2 rabbit polyclonal antibodies (antibody 52, 1:2000), and anti-synapsin mouse monoclonal antibodies (Synaptic Systems, 1:1000). Alexa-Fluor 546 anti-mouse and Alexa-Fluor 633 anti-rabbit secondary antibodies were used for detection. Images were acquired with a Leica TCS2 confocal microscope with identical settings applied to all samples in an experiment. Single confocal sections were recorded at 1 airy unit pinhole.

Munc13-1 Knockdown

The Munc13-1 KD sequence (KD91, GCCTGAGATCTTCGAGCTTAT) was expressed from an H1 promotor sequence in a lentiviral vector and was followed by a ubiquitin promoter-driven mCherry. Munc13-deficient neurons were generated by Munc13-1 knockdown in Munc13-2 constitutive knockout neurons (Varoqueaux et al., 2002). Munc13-2 knockout neurons expressing mCherry but not Munc13-1 KD shRNA were used as control neurons.

Miscellaneous

SDS/PAGE gels and immunoblotting were done according to standard methods described in the Supplemental Information (Kaeser et al., 2009; Kaeser et al., 2008). In all experiments, the experimenter was blind to the condition and/or genotype. All animal experiments were performed according to institutional guidelines. All data are shown as means ± standard error of the mean (SEM). Statistical significance was determined by one-way analysis of variance (ANOVA) (electrophysiological recordings) or Student's t test (all other experiments). All numerical and statistical values and the tests used can be found in the Tables S1–S8.

SUPPLEMENTAL INFORMATION

Supplemental Information includes Supplemental Experimental Procedures, eight figures and eight tables and can be found with this article online at doi:10.1016/j.neuron.2011.01.005.

ACKNOWLEDGMENTS

We thank H. Ly for technical assistance, Dr. Nils Brose for the gift of Munc13-antibodies and Munc13-2 KO mice, Dr. Z. Pang for the ubMunc13-2$^{\Delta C2A}$ construct, and members of the Südhof lab for comments. This work was supported by grants from the National Institites of Health (NINDS 33564 to T.C.S., DA029044 to P.S.K.), and by a Swiss National Science Foundation Postdoctoral Fellowship (to P.S.K.).

Accepted: January 8, 2011
Published: January 26, 2011

REFERENCES

Andrews-Zwilling, Y.S., Kawabe, H., Reim, K., Varoqueaux, F., and Brose, N. (2006). Binding to Rab3A-interacting molecule RIM regulates the presynaptic recruitment of Munc13-1 and ubMunc13-2. J. Biol. Chem. *281*, 19720–19731.

Augustin, I., Rosenmund, C., Südhof, T.C., and Brose, N. (1999a). Munc13-1 is essential for fusion competence of glutamatergic synaptic vesicles. Nature *400*, 457–461.

Augustin, I., Betz, A., Herrmann, C., Jo, T., and Brose, N. (1999b). Differential expression of two novel Munc13 proteins in rat brain. Biochem. J. *337*, 363–371.

Basu, J., Shen, N., Dulubova, I., Lu, J., Guan, R., Guryev, O., Grishin, N.V., Rosenmund, C., and Rizo, J. (2005). A minimal domain responsible for Munc13 activity. Nat. Struct. Mol. Biol. *12*, 1017–1018.

Betz, A., Okamoto, M., Benseler, F., and Brose, N. (1997). Direct interaction of the rat unc-13 homologue Munc13-1 with the N terminus of syntaxin. J. Biol. Chem. *272*, 2520–2526.

Betz, A., Thakur, P., Junge, H.J., Ashery, U., Rhee, J.S., Scheuss, V., Rosenmund, C., Rettig, J., and Brose, N. (2001). Functional interaction of the active zone proteins Munc13-1 and RIM1 in synaptic vesicle priming. Neuron *30*, 183–196.

Brose, N., Hofmann, K., Hata, Y., and Südhof, T.C. (1995). Mammalian homologues of Caenorhabditis elegans unc-13 gene define novel family of C2-domain proteins. J. Biol. Chem. *270*, 25273–25280.

Calakos, N., Schoch, S., Südhof, T.C., and Malenka, R.C. (2004). Multiple roles for the active zone protein RIM1alpha in late stages of neurotransmitter release. Neuron *42*, 889–896.

Castillo, P.E., Janz, R., Südhof, T.C., Tzounopoulos, T., Malenka, R.C., and Nicoll, R.A. (1997). Rab3A is essential for mossy fibre long-term potentiation in the hippocampus. Nature *388*, 590–593.

Castillo, P.E., Schoch, S., Schmitz, F., Südhof, T.C., and Malenka, R.C. (2002). RIM1α is required for presynaptic long-term potentiation. Nature *415*, 327–330.

Chevaleyre, V., Heifets, B.D., Kaeser, P.S., Südhof, T.C., and Castillo, P.E. (2007). Endocannabinoid-mediated long-term plasticity requires cAMP/PKA signaling and RIM1α. Neuron *54*, 801–812.

Coppola, T., Magnin-Luthi, S., Perret-Menoud, V., Gattesco, S., Schiavo, G., and Regazzi, R. (2001). Direct interaction of the Rab3 effector RIM with Ca^{2+} channels, SNAP-25, and synaptotagmin. J. Biol. Chem. *276*, 32756–32762.

Dulubova, I., Lou, X., Lu, J., Huryeva, I., Alam, A., Schneggenburger, R., Südhof, T.C., and Rizo, J. (2005). A Munc13/RIM/Rab3 tripartite complex: From priming to plasticity? EMBO J. *24*, 2839–2850.

Fourcaudot, E., Gambino, F., Humeau, Y., Casassus, G., Shaban, H., Poulain, B., and Lüthi, A. (2008). cAMP/PKA signaling and RIM1α mediate presynaptic LTP in the lateral amygdala. Proc. Natl. Acad. Sci. USA *105*, 15130–15135.

Gracheva, E.O., Hadwiger, G., Nonet, M.L., and Richmond, J.E. (2008). Direct interactions between C. elegans RAB-3 and Rim provide a mechanism to target vesicles to the presynaptic density. Neurosci. Lett. *444*, 137–142.

Guan, R., Dai, H., and Rizo, J. (2008). Binding of the Munc13-1 MUN domain to membrane-anchored SNARE complexes. Biochemistry *47*, 1474–1481.

Han, Y., Kaeser, P.S., Sudhof, T.C., and Schneggenburger, R. (2011). RIM determines Ca^{2+} channel density and vesicle docking at the presynaptic active zone. Neuron *69*, this issue, 304–316.

Hibino, H., Pironkova, R., Onwumere, O., Vologodskaia, M., Hudspeth, A.J., and Lesage, F. (2002). RIM binding proteins (RBPs) couple Rab3-interacting molecules (RIMs) to voltage-gated $Ca^{(2+)}$ channels. Neuron *34*, 411–423.

Junge, H.J., Rhee, J.S., Jahn, O., Varoqueaux, F., Spiess, J., Waxham, M.N., Rosenmund, C., and Brose, N. (2004). Calmodulin and Munc13 form a Ca2+ sensor/effector complex that controls short-term synaptic plasticity.). Calmodulin and Munc13 form a Ca2+ sensor/effector complex that controls short-term synaptic plasticity. Cell *118*, 389–401.

Kaeser, P.S., Kwon, H.B., Chiu, C.Q., Deng, L., Castillo, P.E., and Südhof, T.C. (2008). RIM1α and RIM1β are synthesized from distinct promoters of the RIM1 gene to mediate differential but overlapping synaptic functions. J. Neurosci. *28*, 13435–13447.

Kaeser, P.S., Deng, L., Chávez, A.E., Liu, X., Castillo, P.E., and Südhof, T.C. (2009). ELKS2alpha/CAST deletion selectively increases neurotransmitter release at inhibitory synapses. Neuron *64*, 227–239.

Kaeser, P.S., Deng, L., Wang, Y., Dulubova, I., Liu, X., Castillo, P.E., Rizo, J., and Südhof, T.C. (2011). RIM proteins tether Ca^{2+}-channels to presynaptic active zones via a direct PDZ-domain interaction. Cell *144*, this issue, 282–295.

Katz, B. (1969). The Release of Neural Transmitter Substances (Liverpool: Liverpool Univ Press).

Kiyonaka, S., Wakamori, M., Miki, T., Uriu, Y., Nonaka, M., Bito, H., Beedle, A.M., Mori, E., Hara, Y., De Waard, M., et al. (2007). RIM1 confers sustained activity and neurotransmitter vesicle anchoring to presynaptic Ca^{2+} channels. Nat. Neurosci. *10*, 691–701.

Ko, J., Na, M., Kim, S., Lee, J.R., and Kim, E. (2003). Interaction of the ERC family of RIM-binding proteins with the liprin-α family of multidomain proteins. J. Biol. Chem. *278*, 42377–42385.

Koch, H., Hofmann, K., and Brose, N. (2000). Definition of Munc13-homology-domains and characterization of a novel ubiquitously expressed Munc13 isoform. Biochem. J. *349*, 247–253.

Koushika, S.P., Richmond, J.E., Hadwiger, G., Weimer, R.M., Jorgensen, E.M., and Nonet, M.L. (2001). A post-docking role for active zone protein Rim. Nat. Neurosci. *4*, 997–1005.

Lu, J., Machius, M., Dulubova, I., Dai, H., Südhof, T.C., Tomchick, D.R., and Rizo, J. (2006). Structural basis for a Munc13-1 homodimer to Munc13-1/RIM heterodimer switch. PLoS Biol. *4*, e192.

Madison, J.M., Nurrish, S., and Kaplan, J.M. (2005). UNC-13 interaction with syntaxin is required for synaptic transmission. Curr. Biol. *15*, 2236–2242.

Maximov, A., Pang, Z.P., Tervo, D.G., and Südhof, T.C. (2007). Monitoring synaptic transmission in primary neuronal cultures using local extracellular stimulation. J. Neurosci. Methods *161*, 75–87.

Maximov, A., Tang, J., Yang, X., Pang, Z.P., and Südhof, T.C. (2009). Complexin controls the force transfer from SNARE complexes to membranes in fusion. Science *323*, 516–521.

Mishra, P., Socolich, M., Wall, M.A., Graves, J., Wang, Z., and Ranganathan, R. (2007). Dynamic scaffolding in a G protein-coupled signaling system. Cell *131*, 80–92.

Mittelstaedt, T., Alvaréz-Baron, E., and Schoch, S. (2010). RIM proteins and their role in synapse function. Biol. Chem. *391*, 599–606.

Moulder, K.L., and Mennerick, S. (2005). Reluctant vesicles contribute to the total readily releasable pool in glutamatergic hippocampal neurons. J. Neurosci. *25*, 3842–3850.

Ohtsuka, T., Takao-Rikitsu, E., Inoue, E., Inoue, M., Takeuchi, M., Matsubara, K., Deguchi-Tawarada, M., Satoh, K., Morimoto, K., Nakanishi, H., and Takai, Y. (2002). Cast: A novel protein of the cytomatrix at the active zone of synapses that forms a ternary complex with RIM1 and munc13-1. J. Cell Biol. *158*, 577–590.

Pawson, C.T., and Scott, J.D. (2010). Signal integration through blending, bolstering and bifurcating of intracellular information. Nat. Struct. Mol. Biol. *17*, 653–658.

Rosenmund, C., and Stevens, C.F. (1996). Definition of the readily releasable pool of vesicles at hippocampal synapses. Neuron *16*, 1197–1207.

Rosenmund, C., Sigler, A., Augustin, I., Reim, K., Brose, N., and Rhee, J.S. (2002). Differential control of vesicle priming and short-term plasticity by Munc13 isoforms. Neuron *33*, 411–424.

Schoch, S., Castillo, P.E., Jo, T., Mukherjee, K., Geppert, M., Wang, Y., Schmitz, F., Malenka, R.C., and Südhof, T.C. (2002). RIM1α forms a protein scaffold for regulating neurotransmitter release at the active zone. Nature *415*, 321–326.

Schoch, S., Mittelstaedt, T., Kaeser, P.S., Padgett, D., Feldmann, N., Chevaleyre, V., Castillo, P.E., Hammer, R.E., Han, W., Schmitz, F., et al. (2006). Redundant functions of RIM1α and RIM2α in $Ca^{(2+)}$-triggered neurotransmitter release. EMBO J. *25*, 5852–5863.

Shin, O.H., Lu, J., Rhee, J.S., Tomchick, D.R., Pang, Z.P., Wojcik, S.M., Camacho-Perez, M., Brose, N., Machius, M., Rizo, J., et al. (2010). Munc13 C2B domain is an activity-dependent Ca2+ regulator of synaptic exocytosis.).Munc13 C2B domain is an activity-dependent Ca2+ regulator of synaptic exocytosis. Nat. Struct. Mol. Biol. *17*, 280–288.

Siksou, L., Varoqueaux, F., Pascual, O., Triller, A., Brose, N., and Marty, S. (2009). A common molecular basis for membrane docking and functional priming of synaptic vesicles. Eur. J. Neurosci. *30*, 49–56.

Stevens, C.F. (2003). Neurotransmitter release at central synapses. Neuron *40*, 381–388.

Stevens, D.R., Wu, Z.X., Matti, U., Junge, H.J., Schirra, C., Becherer, U., Wojcik, S.M., Brose, N., and Rettig, J. (2005). Identification of the minimal protein domain required for priming activity of Munc13-1. Curr. Biol. *15*, 2243–2248.

Südhof, T.C. (2004). The synaptic vesicle cycle. Annu. Rev. Neurosci. *27*, 509–547.

Varoqueaux, F., Sigler, A., Rhee, J.S., Brose, N., Enk, C., Reim, K., and Rosenmund, C. (2002). Total arrest of spontaneous and evoked synaptic transmission but normal synaptogenesis in the absence of Munc13-mediated vesicle priming. Proc. Natl. Acad. Sci. USA *99*, 9037–9042.

Wang, Y., and Südhof, T.C. (2003). Genomic definition of RIM proteins: Evolutionary amplification of a family of synaptic regulatory proteins(small star, filled). Genomics *81*, 126–137.

Wang, Y., Okamoto, M., Schmitz, F., Hofmann, K., and Südhof, T.C. (1997). Rim is a putative Rab3 effector in regulating synaptic-vesicle fusion. Nature *388*, 593–598.

Wang, Y., Sugita, S., and Südhof, T.C. (2000). The RIM/NIM family of neuronal C2 domain proteins. Interactions with Rab3 and a new class of Src homology 3 domain proteins. J. Biol. Chem. *275*, 20033–20044.

Wang, Y., Liu, X., Biederer, T., and Südhof, T.C. (2002). A family of RIM-binding proteins regulated by alternative splicing: Implications for the genesis of synaptic active zones. Proc. Natl. Acad. Sci. USA *99*, 14464–14469.

Weimer, R.M., Gracheva, E.O., Meyrignac, O., Miller, K.G., Richmond, J.E., and Bessereau, J.L. (2006). UNC-13 and UNC-10/rim localize synaptic vesicles to specific membrane domains. J. Neurosci. *26*, 8040–8047.

Wojcik, S.M., and Brose, N. (2007). Regulation of membrane fusion in synaptic excitation-secretion coupling: Speed and accuracy matter. Neuron *55*, 11–24.

Wu, L.G., and Borst, J.G. (1999). The reduced release probability of releasable vesicles during recovery from short-term synaptic depression. Neuron *23*, 821–832.

Xu-Friedman, M.A., Harris, K.M., and Regehr, W.G. (2001). Three-dimensional comparison of ultrastructural characteristics at depressing and facilitating synapses onto cerebellar Purkinje cells. J. Neurosci. *21*, 6666–6672.